Singlet Order Conversion and Parahydrogen-Induced Hyperpolarization of ^{13}C Nuclei in Near-Equivalent Spin Systems

James Eills[a], Gabriele Stevanato[a], Christian Bengs[b], Stefan Glöggler[a], Stuart J. Elliott[a], Javier Alonso-Valdesueiro[a], Giuseppe Pileio[a] and Malcolm H. Levitt[a]*

Abstract: *We have demonstrated two radiofrequency pulse methods which convert the nuclear singlet order of proton spin pairs into the magnetisation of nearby ^{13}C nuclei. These irradiation schemes work well in the near-equivalence regime of the three-spin system, which applies when the difference in the two ^{1}H-^{13}C couplings is much smaller than the ^{1}H-^{1}H coupling. We use pulse sequences to generate thermally polarized singlet states in a reproducible manner, and study the singlet-to-magnetisation transfer step. Preliminary results demonstrate a parahydrogen-enhanced ^{13}C polarisation level of at least 9%, providing a signal enhancement factor of more than 9000, using 50% enriched parahydrogen.*

Introduction

Hyperpolarized substances display greatly enhanced nuclear spin order, giving rise to nuclear magnetic resonance (NMR) signals enhanced by up to 5 orders of magnitude relative to standard thermal polarisation. The large signal enhancement enables important applications such as the *in vivo* characterisation of human cancer[1]. In parahydrogen-induced polarisation (PHIP), the hyperpolarized substances are generated by chemical reactions of hydrogen gas which has been enriched in the *para* spin isomer[2-18]. PHIP may be used to generate small ^{13}C-labelled molecules in a hyperpolarized state, with many potential applications in molecular imaging[7-10,18].

Hydrogenation reactions with para-enriched hydrogen yield a product displaying strongly enhanced nuclear *singlet order*, meaning a population difference between the singlet state and the triplet manifold[19].

Singlet order is an example of a *long-lived state* (LLS), with a relaxation time longer than the spin-lattice relaxation time constant T_1 which governs the decay of ordinary nuclear magnetisation[20,21]. Techniques have been developed for converting nuclear magnetisation into long-lived singlet order, and *vice versa*.[20-25] For example, the SLIC (spin-lock-induced crossing)[25-29] and M2S/S2M (magnetisation-to-singlet/singlet-to-magnetisation)[22,30-32] methods are designed to operate in the *near-equivalence regime*, in which the two nuclei involved in the singlet state have a much larger spin-spin coupling than any interactions which break exchange symmetry, such as a chemical shift difference between the two spins, or asymmetric couplings to a third nucleus.

When PHIP is used for ^{13}C magnetisation enhancement, it is necessary to convert hyperpolarized proton singlet order into nuclear magnetisation of a different spin species. One promising concept involves *side-arm hydrogenation*, in which a desired substrate is chemically bonded to a side arm able to react with para hydrogen; the enhanced polarization transferred via para hydrogenation is then converted to spin polarization at one (or more) site of the substrate before chemical cleavage of the side arm to liberate the hyperpolarized agent.[3-5] A series of techniques have been developed for the transformation of singlet order into heteronuclear magnetisation. These include field switching and resonant radiofrequency pulse sequences[3-17]. The first pulse sequences of this kind were developed by Goldman and co-workers[9] but are not well-suited to the important near-equivalence regime relevant to the promising sidearm-hydrogenation procedures.[3-5] Kadlecek and co-workers proposed a set of more general solutions[11].

In this paper we demonstrate that the techniques developed in the field of long-lived states may be applied to the problem of converting singlet order into heteronuclear magnetisation. The SLIC method may be applied almost directly, while the S2M sequence may be adapted by changing the pulse sequence loop numbers and definition of the echo delay. These sequences are relatively short, only involve radiation on a single radiofrequency channel, and provide an efficient transfer of nuclear singlet order into heteronuclear magnetisation, in the near-equivalence regime. Furthermore, the S2hM (singlet-to-heteronuclear-magnetisation) method is well-compensated for resonance offset, without the addition of extra 180° pulses.

In the first part of the next section we show results for singlet NMR techniques, applied to thermally polarized nuclear spin systems, to generate nuclear singlet order. The amount of singlet polarization generated this way is many orders of magnitude smaller than when parahydrogen is used. However, the thermal procedures are fully reproducible and allow a robust characterisation of the conversion process from proton singlet order to ^{13}C magnetization by removing chemical reaction rates from the dynamics. We use a simple test system (natural abundance ^{13}C in fumaric acid) to explore the behaviour of the SLIC and S2hM sequences, and compare these methods to some previously-described procedures in the near-equivalence context. In the second part of the results section, a preliminary demonstration of parahydrogen-induced polarization of ^{13}C nuclei using the SLIC method is given. The theory section provides the quantum theory of the SLIC methods in this 3-spin-1/2 context. The appendix provides the definitions of the polarizations used in this paper, and discusses the associated operators.

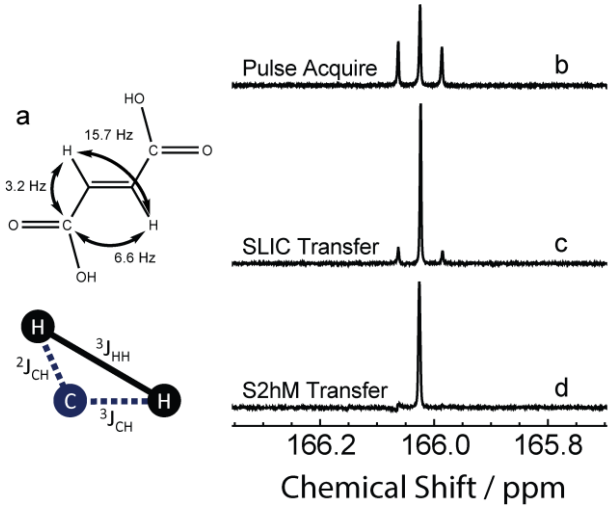

Figure 1: (a) Molecular structure of fumaric acid showing the J-couplings in the 1-^{13}C isotopomer.
(b) ^{13}C spectrum obtained by a single $(\pi/2)_x$ ^{13}C pulse, showing the 1:2:1 triplet associated with a near-equivalent AA'X system.
(c) ^{13}C spectrum obtained using the pulse sequence in Figure 2(a), with proton singlet order converted into ^{13}C magnetisation by the SLIC pulse.
(d) ^{13}C spectrum obtained using the pulse sequence in Figure 2(b), with proton singlet order converted into ^{13}C magnetisation by the S2hM pulse sequence. All spectra show the carbonyl spectral region and were obtained with 64 transients, acquired at a magnetic field of 11.7 T. No ^{1}H decoupling was used during data acquisition. A phase shift of $\pi/2$ was applied to spectra (b) and (c) relative to spectrum (d).

Results and Discussions

Most of the results shown below were obtained on an unlabelled sample of 0.86 M fumaric acid in degassed dimethyl sulfoxide DMSO-d_6 (Figure 1a). All experiments studied the ^{13}C NMR signals from the naturally occurring ~2% of fumaric acid molecules with a ^{13}C nucleus at the carboxylic acid site (1-^{13}C). This isotopomer comprises a AA'X spin system of two chemically equivalent protons and one ^{13}C, with a ^{1}H-^{1}H J-coupling of $^{3}J_{HH}$ = 15.7 ± 0.4 Hz.

The ordinary ^{13}C NMR spectrum without ^{1}H decoupling, shown in Figure 1(b), displays a 1:2:1 triplet structure, with the peak splitting given by the mean of the two ^{1}H-^{13}C J-couplings, ($^{2}J_{CH}$+$^{3}J_{CH}$)/2 = 4.9 ± 0.3 Hz.

This paper is mainly concerned with the near-equivalence regime, which is defined as $\theta \leq 30°$, where $\theta = \arctan(\Delta J_{CH}/2J_{HH})$ (note: some workers in the field use the angle $\theta_G = \pi/2 - \theta$). The couplings in fumaric acid give $\theta = 6.2°$, which makes it a convenient test system for evaluating pulse sequences to mimic polarization transfer across a large number of bonds. In this regime, it is not possible to determine the $^{2}J_{CH}$ and $^{3}J_{CH}$ couplings individually from the NMR spectrum. The difference between the heteronuclear couplings ΔJ_{CH} = $^{2}J_{CH}$ - $^{3}J_{CH}$ = 3.4 ± 0.3 Hz was estimated by data from the singlet NMR experiments (see below). The estimates of the individual heteronuclear couplings are therefore $^{2}J_{CH}$ = 3.2 ± 0.2 Hz and $^{3}J_{CH}$ = 6.6 ± 0.2 Hz. It should be noted that the methods described here provide a useful way of estimating J-couplings in the near-equivalence regime.

Previous experimental work on the conversion of proton singlet order into heteronuclear magnetisation employed parahydrogen reactions to generate singlet order, which makes quantification difficult. For the present work we generated proton singlet order in a reproducible manner from thermal equilibrium proton magnetisation, using techniques developed in the context of LLS[20-32].

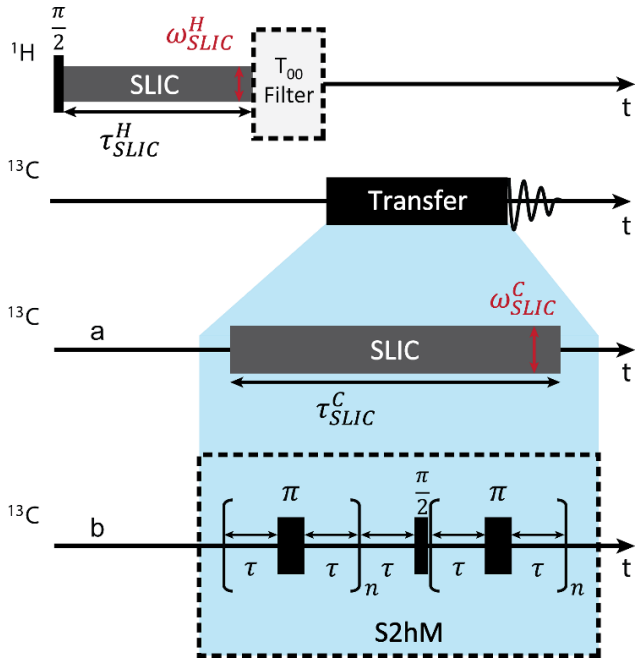

Figure 2: Pulse sequence for characterising the transformation of ^{1}H singlet order into ^{13}C magnetisation. A SLIC sequence on the proton channel generates singlet order, followed by a T_{00} filter to remove any signals not passing through singlet order. The transformation of proton singlet order into ^{13}C magnetisation is achieved by:
a) A SLIC pulse on the ^{13}C channel applied on resonance with the target ^{13}C site.
b) An S2hM pulse sequence using strong, non-selective, pulses on the ^{13}C channel, separated by delays. In practice, composite π pulses are used.

The pulse sequences are shown in Figure 2. Singlet order is generated on the protons by applying a SLIC pulse sequence at the proton resonance frequency. The radiofrequency field amplitude is set to match the proton nutation frequency with the proton-proton J-coupling $\omega^{H}_{SLIC} = 2\pi J_{HH}$. This condition establishes a resonance, in which the difference between the two ^{1}H-^{13}C J-couplings drives oscillations from proton magnetisation into proton singlet order. As shown in the Theory section, the amplitude of the proton singlet order is proportional to $\sin^2(\pi \Delta J_{CH} \tau^{H}_{SLIC}/2\sqrt{2})$, in the absence of relaxation and other imperfections, and is maximised at $\tau^{H}_{SLIC} = \sqrt{2}/\Delta J_{CH}$ (described further in the Theory section).

The ^{1}H SLIC sequence is followed by a "T_{00} filter", used to suppress NMR signals not passing through proton singlet order[33] (see the Supporting Information). This is the sequence [G_1]-$90_{54.7°}$-[G_2]-$90_{54.7°}90_{180°}$-[G_3]. G_1, G_2 and G_3 are z pulsed-field-gradients with a sine-bell shape. The relative strengths were 10, -10 and -15 G cm^{-1}, and the durations were 8.8, 4.8 and 4.0 ms.

We employed two different methods for converting the proton singlet order into ^{13}C magnetisation, both of which operate in the near-equivalence regime and only employ radiofrequency (rf) irradiation on the ^{13}C channel.

1. SLIC method (Figure 2a). A weak unmodulated rf field is applied at the resonance frequency of the "target" ^{13}C site. If the amplitude of the ^{13}C field is such that the ^{13}C nutation frequency matches the ^{1}H-^{1}H J-coupling $\omega^{C}_{SLIC} = 2\pi J_{HH}$, proton singlet order oscillates into transverse ^{13}C magnetisation, locked in the opposite direction to the rf field. In the absence of relaxation and other imperfections, the amplitude of transverse ^{13}C magnetisation is proportional to $\sin^2(\pi \Delta J_{CH} \tau^{C}_{SLIC}/2)$, so that the ^{13}C magnetisation yield is optimised after an interval $\tau^{C}_{SLIC} = 1/\Delta J_{CH}$ (see the Theory section). A similar conversion procedure (albeit in a 4-spin system) is used in high-field SABRE (signal amplification by reversible exchange) experiments[27].

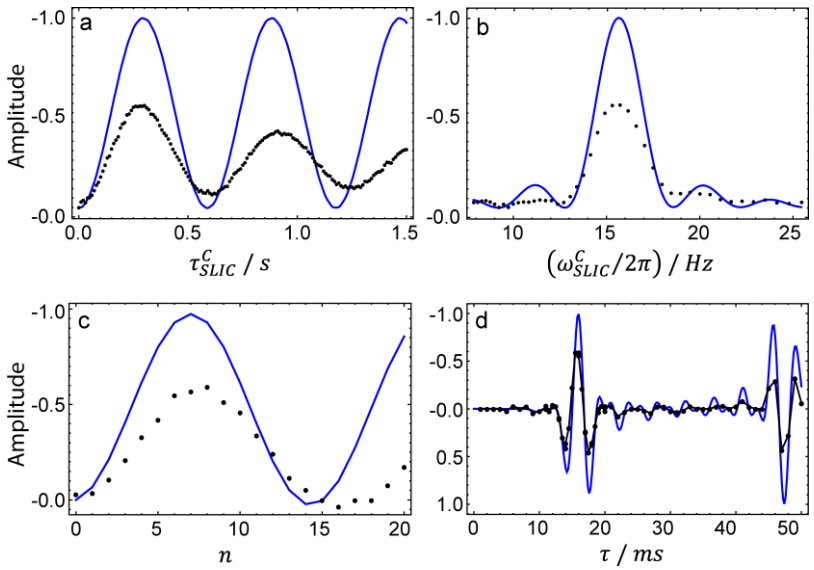

Figure 3: Amplitudes for the conversion of proton singlet polarization into ^{13}C Zeeman polarization in 1-^{13}C-fumaric acid: simulations (solid blue lines) and experimental results (black points). The vertical scale in all plots is normalised such that 1 corresponds to 100% conversion from proton singlet order into ^{13}C polarization. A conversion amplitude of 1 indicates that pure parahydrogen, if reacted without loss, would give rise to fully polarized ^{13}C nuclei. All amplitudes are negative to indicate magnetisation generated opposite to the pulse phase. The best-case transfer amplitude was 54.0% for SLIC and 59.3% for S2hM.
(a) SLIC pulse sequence as a function of SLIC duration τ^C_{SLIC} with a fixed amplitude $\omega^C_{SLIC}/2\pi = 15.7$ Hz.
(b) SLIC pulse sequence as a function of ^{13}C nutation frequency with a fixed duration $\tau^C_{SLIC} = 280$ ms.
(c) S2hM pulse sequence as a function of loop number n, with delay τ fixed at 15.8 ms.
(d) S2hM pulse sequence as a function of delay τ, with loop number n=7 . Each experimental point is a result of 4 transients, using a delay between transients of 60 s.

Experimental results showing the oscillatory transfer of proton singlet order into transverse ^{13}C magnetisation under the ^{13}C SLIC sequence are shown in Figure 3(a). The data points were obtained by repeating the pulse sequence in Figure 2(a) for different ^{13}C SLIC durations. The experimental data points were normalised by calibration experiments, such that a value of 1 would correspond to 100% conversion of proton singlet polarization into ^{13}C Zeeman polarization, as described in the Appendix. An optimal transfer amplitude of 54.0% is obtained at a SLIC duration $\tau^C_{SLIC} = 280$ ms.
The experimental polarization conversion amplitude for SLIC, as derived from the spectral integral, is plotted against ^{13}C rf amplitude (expressed as a nutation frequency) in Figure 3(b). This shows a distinct peak at 15.7 Hz, corresponding to the match of ω^C_{SLIC} with $2\pi J_{HH}$.
The ^{13}C NMR spectrum, obtained by the pulse sequence in Figure 2(a) using a ^{13}C SLIC pulse of duration 280 ms, is shown in Figure 1(c). The weak outer components of the ^{1}H-coupled ^{13}C multiplet are in agreement with the theory of the SLIC singlet-to-magnetisation transfer process. The singlet order between the protons is converted predominantly into ^{13}C coherences involving the ^{1}H singlet state and the central ^{1}H triplet state, both of which make up the central peak of the ^{13}C multiplet.
Numerical simulations of the conversion amplitudes, using the SpinDynamica software platform[34], are shown by solid blue lines in Figure 3.
2. S2hM sequence (Figure 2b). The *homonuclear* singlet-to-magnetisation (S2M) sequence[22,30-32] comprises a strong $\pi/2$ pulse and a delay, on either side of two π pulse echo trains, with the second echo train being twice as long as the first. The S2M sequence is adapted to perform *heteronuclear* singlet-to-magnetization transfer by making the two echo trains equal in repetition number, as depicted in Figure 2(b). We refer to this sequence as S2hM (singlet-to-heteronuclear-magnetisation).
The theoretical values of the intervals τ and loop numbers n are given by

$$\tau = 1/\left(4\sqrt{J_{HH}^2 + (\Delta J_{CH}/2)^2}\right) \quad (1)$$

$$n = \text{round}\left(\pi/\left(4\arctan(\Delta J_{CH}/2J_{HH})\right)\right) \quad (2)$$

The S2hM sequence converts proton singlet order into heteronuclear magnetisation in a near-equivalent 3-spin-1/2 system, with a near-100% theoretical conversion amplitude. Although the S2hM sequence is a factor of $\sim\pi/2$ longer than SLIC, it is more robust with respect to resonance offset and magnetic field homogeneity, especially when composite π pulses are used[35].
Figure 3 (c) and (d) show experimental conversion amplitudes for proton singlet order into transverse ^{13}C magnetisation using the S2hM sequence, as a function of the echo interval τ and loop number n. An optimal transfer amplitude of the conversion step of 59.3% was obtained for echo interval τ = 15.8 ms and loop number n = 7 (see Supporting Information).
The ^{13}C NMR spectrum, obtained by the pulse sequence in Figure 2(b) using an S2hM sequence on the ^{13}C channel, is shown in Figure 1(b). The spectrum has a similar appearance to that obtained using SLIC.
The SLIC and S2hM sequences are both efficient in converting proton singlet order into heteronuclear magnetisation, in the near-equivalence regime, where $\theta \leq 30°$. Two other sequences known to the authors work well in this regime: Kadlecek Case 2b[11], called here K2b, and a modified Goldman sequence which incorporates a number of "pumping pulses" to build up magnetization on the target nucleus[15]. These hard-pulse sequences work similarly to S2hM, but have more adjustable delay periods, which is advantageous when θ is near 30°. For comparison, these two hard-pulse sequences were also applied to fumaric acid in the same way as S2hM and SLIC, and give transfer amplitudes of 50.2% (Goldman) and 54.5% (K2b). The complete sequences are given in the Supp. Info. For all four sequences explored here, the correspondence of experimental results with simulations is acceptable, except for an additional loss in experimental signal

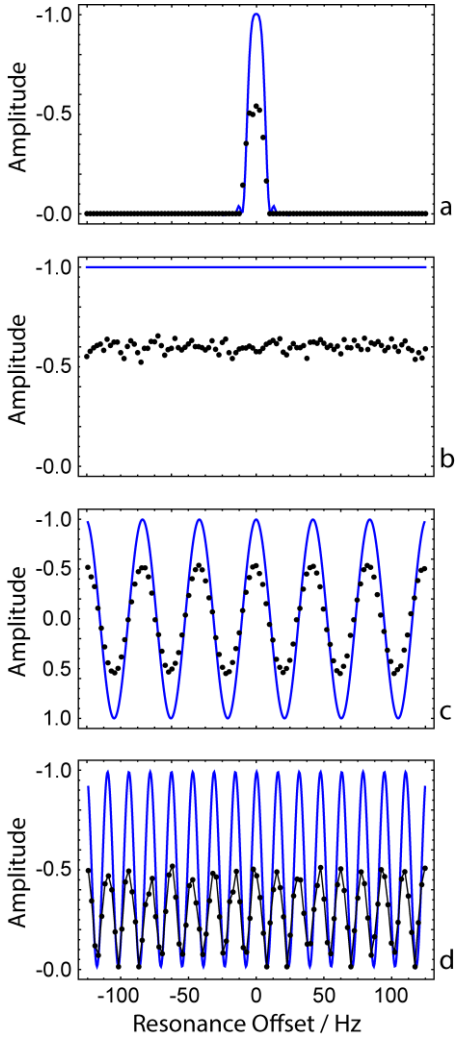

Figure 4: Conversion amplitudes as a function of resonance offset from the target carbon resonance in 1-^{13}C-fumaric acid: simulations (solid blue lines) and experimental results (black points). The vertical scale is the same as in Figure 3.
(a) SLIC pulse sequence using amplitude $\omega^C_{SLIC}/2\pi$=15.7 Hz and duration τ^C_{SLIC}= 280ms.
(b) S2hM pulse sequence using delay τ=15.8 ms and loop number n=7.
(c) Kadlecek pulse sequence using delays $\tau_{1,2,3}$=31.6 and τ_4=7.9 ms, with loop number n=5. A complete sequence is shown in the Supp. Info.
(d) Goldman pulse sequence using delays $\tau_{0,1,3,4}$=31.6 and τ_4=15.8 ms, with loop numbers n_1=5 and n_2=7. A complete sequence is shown in the Supp. Info.

strength observed, presumably associated with relaxation and rf inhomogeneity. The detailed reasons for the loss in conversion efficiency are not yet completely understood.
A favourable feature of SLIC is its high rate of transfer. In the near-equivalence limit, the duration of the SLIC method required to provide complete transfer is a factor of $2/\pi$ shorter than S2hM, K2b and modified Goldman schemes. SLIC performs the transfer on fumaric acid in 280 ms, compared to the 460 ms required for the hard-pulse methods.
Some applications of these pulse sequences involve manipulations of the spins in a low magnetic field, in order to minimize proton chemical shift. Low-field electromagnets often have a limited field homogeneity and suffer from instability and drift. The performance of these methods in the presence of a frequency mismatch between the applied rf frequency and the Larmor frequency of the spins (resonance offset) is therefore an important characteristic. Figure 4 shows the performance of the singlet-to-magnetization procedures as a function of resonance offset. Although these data were obtained on fumaric acid in high field, they provide valuable information on the performance of the same pulse sequences in the low-field context.
Figure 4a shows the resonance offset performance of the SLIC sequence. The method is highly sensitive to resonance offset, as expected for a weak rf field. Figure 4b shows that S2hM, on the other hand, is highly robust with respect to resonance offset. The Kadlecek and Goldman sequences display a strongly oscillatory transfer with respect to resonance offset (Figure 4c and d). For example, the conversion amplitude of the K2b sequence changes sign every ~21 Hz, which corresponds to a field difference of ~2 μT. These sequences may be offset-compensated by including two pairs of 180° pulses on both the ^{13}C and ^{1}H channels in every pulse sequence delay[8,15], but this adds much complexity and presumably gives rise to additional losses due to pulse imperfections.

Parahydrogen-Induced Polarization
In Figure 5, we show a preliminary result demonstrating parahydrogen-induced ^{13}C NMR signal enhancement on the molecule dimethyl maleate. The J_{HH} coupling for this molecule is known to be 11.6 Hz[29], and we make the assumption the ΔJ_{CH} value is approximately the same as we determined for maleic acid, 10.5 Hz. This would mean the spin system has a relatively high θ value for a molecule in the near-equivalence limit of $\theta = \sim 24°$, but it serves as a useful model system for obtaining preliminary results. We enriched H_2 gas in the parahydrogen spin isomer by passing it over a charcoal catalyst at 77 K. This was bubbled for 15 s into a solution of 5 mM dimethyl acetylene dicarboxylate-d_6 and 30 mM Rh(dppb)(COD) (hydrogenation catalyst, dppb=diphenylphosphino butane, COD=cyclooctadiene), dissolved in acetone-d_6, at room temperature in an NMR tube already loaded in the high-field (11.7 T) magnet. Immediately after bubbling, a ^{13}C SLIC pulse of duration 95 ms was applied. The Fourier transform of one ^{13}C signal transient is shown in Figure 5(a).
After the reaction had completed, an attempt was made to acquire the unenhanced ^{13}C spectrum by acquiring 1024 single-pulse transients using 90 ° pulses separated by a relaxation interval of 60 s. The signal could not be detected, as shown in Figure 5(b). Independent experiments determined the ^{13}C T_1 of the carbonyl site to be 44 s. We estimate that the parahydrogen-induced signal enhancement in Figure 4a was at least 9000, corresponding to a ^{13}C polarization level of more than 9%. This estimate takes into account a signal loss of ~23% in the unenhanced spectrum due to partial saturation by the 90 ° pulses[36], and was later confirmed by comparing the hyperpolarized peak intensity to that of a ^{13}C-labelled standard (boc-gly-OH-1-^{13}C). A further enhancement by a factor of ~3 would be available by enriching the H_2 gas with parahydrogen at a temperature of 25 K instead of 77 K.
The demonstration in Figure 5 was performed on a molecular system in which the relevant isotopomer of the reaction product contains only three spins-1/2 (neglecting the deuterons), with identical proton chemical shifts. The same procedure could be performed on more general molecules in low magnetic field, so that any chemical shift difference between the protons becomes unimportant.

Theory

In this section we present the quantum theory of the Spin-Lock Induced Crossing (SLIC) procedures, as shown in Figure 2a. The principles of the S2hM sequence will be presented in a separate paper.

Singlet and Zeeman Polarization
One of our aims in this paper is to connect the singlet NMR of thermally polarized systems with the field of parahydrogen-enhanced NMR. For this purpose we now discuss the definitions of polarization levels, and the associated quantum operators used in spin-dynamical calculations and theory.
The term polarization is commonly used in NMR to denote the degree of alignment of nuclear spin magnetic moments with an external axis, typically the external magnetic field. For isolated spins-1/2 with Zeeman eigenstates $|\alpha\rangle$ and $|\beta\rangle$, representing spin

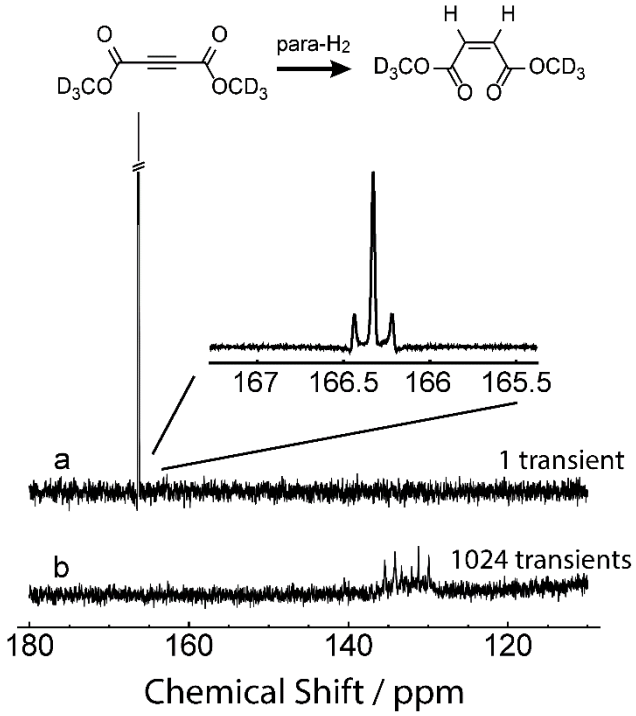

Figure 5: ^{13}C NMR spectra of the COO site of dimethyl maleate-d_6, obtained by the catalytic reaction of the dimethyl ester of acetylene dicarboxylic acid with para-enriched hydrogen, in the NMR magnet.
a) A ^{13}C spectrum acquired after bubbling the para-enriched hydrogen gas for 15 s and applying a ^{13}C SLIC pulse with duration 95 ms, at the frequency of the ^{13}COO resonance. No proton decoupling was used during signal acquisition.
b) An attempt to acquire the ^{13}C NMR spectrum after completion of the reaction by acquiring 1024 single-pulse transients separated by a delay of 60 s. The catalyst gives rise to the structure around 133 ppm. The vertical scale in (b) has been reduced by 32 so as to equalize the noise. Both (a) and (b) have line broadening of 2.3 Hz applied, but the inset spectrum does not. The NMR signal enhancement factor is approximately 9000.

angular momenta of $+\hbar/2$ and $-\hbar/2$ in the field direction, the Zeeman polarization, denoted here p_z, is given by

$$p_z = \frac{n_\alpha - n_\beta}{n_\alpha + n_\beta} \tag{3}$$

where n_α and n_β are the populations of states $|\alpha\rangle$ and $|\beta\rangle$ respectively. The value of p_z is bounded by ± 1, i.e. $-1 \le p_z \le +1$, with $p_z = +1$ indicating complete alignment of the spin angular momenta along the external field, and $p_z = -1$ indicating complete spin alignment in the opposite direction.
For isolated spins-1/2, the spin density operator $\rho(p_z)$ corresponding to an isolated spin-1/2 ensemble with Zeeman polarization p_z is given by

$$\rho(p_z) = \frac{1}{2}\mathbb{1} + p_z I_z \tag{4}$$

where $\mathbb{1}$ is the unity operator. For an ensemble of N-spin-1/2 systems $\{I_1, I_2 \ldots I_N\}$, in which spins I_1 have a Zeeman polarization p_{1z}, spins I_2 have a Zeeman polarization p_{2z}, etc., (and all polarizations are statistically independent), the corresponding spin density operator is given by

$$\rho(p_{1z}, p_{2z}, \ldots) = \left(\frac{1}{2}\mathbb{1} + p_{1z}I_{1z}\right)\left(\frac{1}{2}\mathbb{1} + p_{2z}I_{2z}\right)\ldots\left(\frac{1}{2}\mathbb{1} + p_{Nz}I_{Nz}\right) \tag{5}$$

The quadratic (and higher order) terms are insignificant for thermally polarized systems with small p-values, but become important at high polarization levels.
Define the *operator amplitude* $\langle A \to B\rangle$ as follows:

$$\langle A \to B\rangle = \frac{\langle B|A\rangle}{\langle B|B\rangle} \tag{6}$$

where the Liouville bracket is defined[37]

$$\langle B|A\rangle = \mathrm{Tr}\{B^\dagger A\} \tag{7}$$

and $B^\dagger$ is the adjoint of A. If the operator A may be expressed as

$$A = aB + (\text{terms orthogonal to } B) \tag{8}$$

then $a = \langle A \to B\rangle$. The operator amplitude $\langle A \to B\rangle$ extracts the coefficient of operator B contained in operator A, by calculating a suitably normalized projection of A onto B.
The Zeeman polarization of spins I_j may be derived from an arbitrary density operator ρ as follows:

$$p_{jz} = \langle \rho \to P_{jz}\rangle \tag{9}$$

where the *Zeeman polarization level operator* P_{jz}, is defined:

$$P_{jz} = 2^{1-N} I_{jz} \tag{10}$$

This corresponds to the operator with coefficient p_{1z} in Equation 5. Equations 9 and 10 provide a rigorous method for deriving the Zeeman polarization level of single spins-1/2 from a general density operator.
The term *polarization level operator* is used here to avoid confusion with the *polarization operator* defined by Ernst and co-workers, which has a different meaning[36].
Polarizations along different axes are constructed in a similar way. For example, the polarization of spins I_j along the x-axis may be derived from the density operator through the operator amplitude $\langle \rho \to P_{jx}\rangle$ where $P_{jx} = 2^{1-N} I_{jx}$.
The mean polarization of several spins may be calculated by applying the operator amplitude construction to the summed polarization level operators, for example:

$$\frac{1}{n}\left(p_{jz} + p_{kz} + \cdots p_{nz}\right) = \langle \rho \to P_{jz} + P_{kz} + \cdots P_{nz}\rangle \tag{11}$$

The definition of the operator amplitude in Equation 6 takes care of the normalization.

Singlet Polarization

Consider now an N-spin-1/2 system in which spin pairs $\{I_j, I_k\}$ possess a degree of singlet order, caused either by manipulations of a thermally polarized spin system, or by the injection of singlet order into the system through a reaction with para-enriched hydrogen. The *singlet polarization* of the spin pair, denoted $p_S^{j,k}$ is defined as the difference between the singlet population and the mean of the triplet state populations. A density operator representing a state with singlet polarization $p_S^{j,k}$ for spin pairs $\{I_j, I_k\}$ is given by

$$\rho\left(p_S^{j,k}\right) = 2^{-N}\mathbb{1} + p_S^{j,k}P_S^{j,k} + \left(\text{operators orthogonal to } P_S^{j,k}\right) \tag{12}$$

where the *singlet polarization level operator*, denoted $P_S^{j,k}$, is defined as follows:

$$P_S^{j,k} = -2^{2-N}\mathbf{I}_j \cdot \mathbf{I}_\mathrm{k} \tag{13}$$

The singlet polarization may be obtained from an arbitrary spin density operator as follows:

$$p_S^{j,k} = \langle \rho \to P_S^{j,k} \rangle \tag{14}$$

in similar fashion to the Zeeman polarization (Equation 9). The singlet polarization is bounded as follows: $-1/3 \le p_S^{j,k} \le +1$, where the maximum value of $+1$ indicates complete singlet polarization (as in pure parahydrogen), and the minimum value of $-1/3$ indicates complete depletion of the singlet state (as in pure orthohydrogen). For example, pure parahydrogen is described by a 2-spin-1/2 density operator ($N = 2$):

$$\rho(\text{pure } \mathrm{pH_2}) = \frac{1}{4}\mathbb{1} - \mathbf{I}_1 \cdot \mathbf{I}_2 \tag{15}$$

and has singlet polarization $p_S = +1$. 50% enriched parahydrogen (as generated by catalytic equilibration at ~77 K) is described by a 2-spin-1/2 density operator ($N = 2$):

$$\rho(50\%\ \mathrm{pH_2}) = \frac{1}{4}\mathbb{1} - \frac{1}{3}\mathbf{I}_1 \cdot \mathbf{I}_2 \tag{16}$$

and has singlet polarization $p_S = +1/3$.
Strong Zeeman polarization is accompanied by the depletion of singlet populations and hence negative singlet order. This is revealed by applying the procedure of Equation 14 to the density operator in Equation 5:

$$p_S^{j,k} = \langle \rho(p_{1z}, p_{2z}, \ldots) \to P_S^{j,k} \rangle = -\frac{1}{3}p_{jz}p_{kz} \tag{17}$$

The generation of singlet order by strong Zeeman polarization has been exploited in the context of dynamic nuclear polarization[38,39].

Thermal Polarization
Spin species at thermal equilibrium in a static magnetic field B_0 and temperature T exhibit Zeeman polarizations of the form

$$p_{jz}^{eq} = \tanh\left\{\frac{\hbar\gamma_j B_0}{2k_B T}\right\} \tag{18}$$

where γ_j is the magnetogyric ratio of species I_j and k_B is the Boltzmann constant. At high temperature $\left(k_B T \gg \left|\hbar\gamma_j B_0\right|\right)$ this simplifies to

$$p_{jz}^{eq} \cong \frac{\hbar\gamma_j B_0}{2k_B T} \tag{19}$$

This is an infamously small number of the order 10^{-5} in most circumstances. Thermal singlet polarization for homonuclear spin pairs is given by $-\left(p_{jz}^{eq}\right)^2/3$, which is of the order 10^{-10} and may be ignored.

SLIC Theory
The Principles of the Spin-Lock-Induced Transfer (SLIC) method have been extensively discussed in the case of a homonuclear spin-1/2 pair, where a chemical shift difference induces singlet-to-magnetization polarization transfer, and vice versa[25,26] and also for heteronuclear 4-spin systems.[27,28,40] Here we present the theory of SLIC for a pair of chemically equivalent protons experiencing differential J-couplings to a third spin of different isotopic type, examining the result of SLIC matching conditions on both spin species. In order to make the connection between thermally polarized singlet NMR and parahydrogen-enhanced NMR we use the polarization definitions presented above.
The spin Hamiltonian for the system of two I-spins-1/2 and one S-spin-1/2, in the presence of resonant rf fields with phase 0, is given in the high-field limit by

$$H = 2\pi J_{12}\mathbf{I}_1 \cdot \mathbf{I}_2 + 2\pi J_{13}I_{1z}S_{3z} + 2\pi J_{23}I_{2z}S_{3z} + \omega_{nut}^{I}(I_{1x} + I_{2x}) + \omega_{nut}^{\mathrm{S}}S_{3x} \tag{20}$$

where the rf field amplitudes for the two species are expressed as nutation frequencies ω_{nut}^{I} and ω_{nut}^{S}. Chemical shift terms have been ignored, implying that the two I-spins are chemically equivalent, or that the static field is sufficiently low that chemical shift frequencies are insignificant. The rf irradiation is assumed to be exactly on-resonant for both channels. The Hamiltonian may be written

$$H = \omega_{II}\mathbf{I}_1 \cdot \mathbf{I}_2 + \omega_{IS}^{\Sigma}\frac{1}{2}(I_{1z} + I_{2z})S_{3z} + \omega_{IS}^{\Delta}\frac{1}{2}(I_{1z} - I_{2z})S_{3z} + \omega_{nut}^{I}(I_{1x} + I_{2x}) + \omega_{nut}^{\mathrm{S}}S_{3x} \tag{21}$$

where $\omega_{II} = 2\pi J_{12}$, $\omega_{IS}^{\Sigma} = 2\pi(J_{13} + J_{23})$ and $\omega_{IS}^{\Delta} = 2\pi(J_{13} - J_{23})$.
The SLIC condition for the I-spins is given by $\omega_{nut}^{I} = \omega_{II}$ and $\omega_{nut}^{S} = 0$, while the SLIC condition for the S-spins is given by $\omega_{nut}^{I} = 0$ and $\omega_{nut}^{S} = \omega_{II}$.
The singlet and triplet states for the two I-spins are defined as follows:

$$|S_0^{12}\rangle = \tfrac{1}{\sqrt{2}}(|\alpha_1\beta_2\rangle - |\beta_1\alpha_2\rangle) \tag{22}$$

$$|T_{+1}^{12}\rangle = |\alpha_1\alpha_2\rangle \tag{23}$$

$$|T_0^{12}\rangle = \tfrac{1}{\sqrt{2}}(|\alpha_1\beta_2\rangle + |\beta_1\alpha_2\rangle) \tag{24}$$

$$|T_{-1}^{12}\rangle = |\beta_1\beta_2\rangle \tag{25}$$

where $|\alpha_1\beta_2\rangle$ indicates a state with angular momentum $+1/2$ for spin I_1, and angular momentum $-1/2$ for spin I_2, along the static magnetic field, etc. A basis for the three-spin system may be constructed from the direct product of the singlet and triplet states for the I-spins, and the Zeeman states $|\alpha_3\rangle$ and $|\beta_3\rangle$ for the S-spin:

$$STZ = \{|S_0^{12}\rangle, |T_{+1}^{12}\rangle, |T_0^{12}\rangle, |T_{-1}^{12}\rangle\} \otimes \{|\alpha_3\rangle, |\beta_3\rangle\} \tag{26}$$

A new basis STX, which is suitable for representing the spin dynamics during SLIC, is defined by rotating each of the STZ basis kets by $\pi/2$ about the y-axis:

$$STX = \{R_y(\pi/2)|1\rangle^{STZ} \cdots R_y(\pi/2)|n\rangle^{STZ}\} \tag{27}$$

where $R_y(\theta) = exp\{-i\theta(I_{1y} + I_{2y} + S_{3y})\}$ and $n = 8$.

I-Spin SLIC

The pulse sequence starts with a $(\pi/2)_y$ pulse applied to the I-spins. The initial thermal equilibrium state of the I-spins may be represented by the density operator $\rho_{eq} = (1/8)\mathbb{1} + p_{Iz}^{eq} P_{Iz}$, where the thermal equilibrium polarization is defined in Equation 19 and the polarization level operator is defined in Equation 10:

$$P_{Iz} = \frac{1}{4}(I_{1z} + I_{2z}) \tag{28}$$

The unity operator is ignored in subsequent calculations. The second term is rotated by the pulse into the operator

$$\rho(0) = p_{Iz}^{eq} P_{Ix} = p_{Iz}^{eq} \frac{1}{4}(I_{1x} + I_{2x}) \tag{29}$$

This is the starting condition for the evolution under the radiofrequency field.

In the case of I-spin SLIC irradiation ($\omega_{nut}^{I} = \omega_{II}$ and $\omega_{nut}^{S} = 0$), the matrix representation of the Hamiltonian in Equation 21, in the basis STX is given by:

$$H_{SLIC(I)} = \frac{1}{4\sqrt{2}} \begin{pmatrix} -3\sqrt{2}\omega_{II} & 0 & 0 & 0 & 0 & -\omega_{IS}^{\Delta} & 0 & \omega_{IS}^{\Delta} \\ 0 & 5\sqrt{2}\omega_{II} & 0 & 0 & -\omega_{IS}^{\Delta} & 0 & \omega_{IS}^{\Sigma} & 0 \\ 0 & 0 & \sqrt{2}\omega_{II} & 0 & 0 & \omega_{IS}^{\Sigma} & 0 & \omega_{IS}^{\Sigma} \\ 0 & 0 & 0 & -3\sqrt{2}\omega_{II} & \omega_{IS}^{\Delta} & 0 & \omega_{IS}^{\Sigma} & 0 \\ 0 & -\omega_{IS}^{\Delta} & 0 & \omega_{IS}^{\Delta} & -3\sqrt{2}\omega_{II} & 0 & 0 & 0 \\ -\omega_{IS}^{\Delta} & 0 & \omega_{IS}^{\Sigma} & 0 & 0 & 5\sqrt{2}\omega_{II} & 0 & 0 \\ 0 & \omega_{IS}^{\Sigma} & 0 & \omega_{IS}^{\Sigma} & 0 & 0 & \sqrt{2}\omega_{II} & 0 \\ \omega_{IS}^{\Delta} & 0 & \omega_{IS}^{\Sigma} & 0 & 0 & 0 & 0 & -3\sqrt{2}\omega_{II} \end{pmatrix} \tag{30}$$

An approximate "secular" form of this matrix may be constructed by removing all off-diagonal elements between non-degenerate diagonal elements:

$$H_{SLIC(I)}^{sec} = \frac{1}{4} \begin{pmatrix} -3\omega_{II} & 0 & 0 & 0 & 0 & 0 & 0 & \omega_{IS}^{\Delta}/\sqrt{2} \\ 0 & 5\omega_{II} & 0 & 0 & 0 & 0 & 0 & 0 \\ 0 & 0 & \omega_{II} & 0 & 0 & 0 & 0 & 0 \\ 0 & 0 & 0 & -3\omega_{II} & 0 & 0 & 0 & 0 \\ 0 & 0 & 0 & 0 & -3\omega_{II} & 0 & 0 & 0 \\ 0 & 0 & 0 & 0 & 0 & 5\omega_{II} & 0 & 0 \\ 0 & 0 & 0 & 0 & 0 & 0 & \omega_{II} & 0 \\ \omega_{IS}^{\Delta}/\sqrt{2} & 0 & 0 & 0 & 0 & 0 & 0 & -3\omega_{II} \end{pmatrix} \tag{31}$$

This approximation is justified if $|\omega_{IS}^{\Delta}| \ll |\omega_{II}|$ and $|\omega_{IS}^{\Sigma}| \ll |\omega_{II}|$, i.e. the near-equivalence regime.

Equation 31 shows that states #1 and #8 of the STX basis are mixed by the spin Hamiltonian. Since state #1 is derived by a $(\pi/2)$ rotation of the state $|S_0^{12}\rangle\otimes|\alpha_3\rangle$, while state #8 is derived by a $(\pi/2)$ rotation of the state $|T_{-1}^{12}\rangle\otimes|\beta_3\rangle$, this mixing allows population transfer between the singlet and triplet states of the I-spins, catalysed by the differential couplings to the S-spin. I-spin magnetisation is therefore converted into I-spin singlet order under the action of the I-spin SLIC pulse.

The evolution of the system from an initial state of I-spin polarization along the rf field is as follows:

$$\rho(t) \simeq p_{Iz}^{eq} exp\{-iH_{SLIC(I)}^{sec} t\} P_{Iz} exp\{+iH_{SLIC(I)}^{sec} t\} \tag{32}$$

where relaxation is neglected. A *SpinDynamica* calculation shows that this is given by

$$\begin{aligned} \rho(t) \simeq & \frac{1}{16} p_{Iz}^{eq} \left\{3 + \cos\left(\frac{\omega_{IS}^{\Delta} t}{2\sqrt{2}}\right)\right\} I_x \\ & + \frac{1}{3} p_{Iz}^{eq} \sin^2\left(\frac{\omega_{IS}^{\Delta} t}{4\sqrt{2}}\right) \mathbf{I}_1 \cdot \mathbf{I}_2 \\ & - \frac{1}{24} p_{Iz}^{eq} \sin^2\left(\frac{\omega_{IS}^{\Delta} t}{4\sqrt{2}}\right) (3I_{1x}I_{2x} - \mathbf{I}_1 \cdot \mathbf{I}_2) \\ & + \frac{1}{4\sqrt{2}} p_{Iz}^{eq} \sin\left(\frac{\omega_{IS}^{\Delta} t}{2\sqrt{2}}\right) (I_{1y} - I_{2y}) S_{3z} \\ & + \frac{1}{2\sqrt{2}} p_{Iz}^{eq} \sin\left(\frac{\omega_{IS}^{\Delta} t}{2\sqrt{2}}\right) (I_{1x}I_{2y} - I_{1y}I_{2x}) S_{3z} \end{aligned} \tag{33}$$

All terms on the right-hand side of Equation 33 are orthogonal. The singlet order generated by the I-spin SLIC sequence is given by

$$p_S^I(t) = \langle \rho(t) \to P_S^I \rangle = -\frac{2}{3} p_{Iz}^{eq} \sin^2\left(\frac{\omega_{IS}^{\Delta} t}{4\sqrt{2}}\right) \tag{34}$$

which has a maximum magnitude of $(2/3)p_{Iz}^{eq}$ at a SLIC duration $\tau_{SLIC}^{I} = \sqrt{2}/|J_{13} - J_{23}|$. For weakly polarized systems, the conversion of $(2/3)$ of the Zeeman polarization into singlet polarization is the best possible, under any unitary transformation[41].

S-Spin SLIC

We now examine the action of the S-spin SLIC pulse on a state of proton singlet order, expressed by the density operator:

$$\rho(\tau_{SLIC}^{I}) = p_S^I P_S^I = -\frac{1}{2} p_S^I \mathbf{I}_1 \cdot \mathbf{I}_2 \tag{35}$$

where p_S^I is the I-spin singlet polarization. In the case where the singlet polarization is generated from thermal I-spin Zeeman polarization by the I-spin SLIC sequence, as described above, this initial polarization is given (in the best case) by

$$p_S^I = -\frac{2}{3} p_{Iz}^{eq} \tag{36}$$

However, if the singlet polarization were generated by an ideal reaction with pure parahydrogen, the singlet polarization would be $p_S^I = 1$.

In the case of S-spin SLIC irradiation ($\omega_{nut}^{S} = \omega_{II}$ and $\omega_{nut}^{I} = 0$), the matrix representation of the Hamiltonian is given by:

$$H_{SLIC(S)} = \frac{1}{4\sqrt{2}}\begin{pmatrix} -\sqrt{2}\omega_{II} & 0 & 0 & 0 & 0 & -\omega_{IS}^{\Delta} & 0 & \omega_{IS}^{\Delta} \\ 0 & 3\sqrt{2}\omega_{II} & 0 & 0 & -\omega_{IS}^{\Delta} & 0 & \omega_{IS}^{\Sigma} & 0 \\ 0 & 0 & 3\sqrt{2}\omega_{II} & 0 & 0 & \omega_{IS}^{\Sigma} & 0 & \omega_{IS}^{\Sigma} \\ 0 & 0 & 0 & 3\sqrt{2}\omega_{II} & \omega_{IS}^{\Delta} & 0 & \omega_{IS}^{\Sigma} & 0 \\ 0 & -\omega_{IS}^{\Delta} & 0 & \omega_{IS}^{\Delta} & -5\sqrt{2}\omega_{II} & 0 & 0 & 0 \\ -\omega_{IS}^{\Delta} & 0 & \omega_{IS}^{\Sigma} & 0 & 0 & -\sqrt{2}\omega_{II} & 0 & 0 \\ 0 & \omega_{IS}^{\Sigma} & 0 & \omega_{IS}^{\Sigma} & 0 & 0 & -\sqrt{2}\omega_{II} & 0 \\ \omega_{IS}^{\Delta} & 0 & \omega_{IS}^{\Sigma} & 0 & 0 & 0 & 0 & -\sqrt{2}\omega_{II} \end{pmatrix} \quad (37)$$

An approximate "secular" form of this matrix may be constructed by removing all off-diagonal elements between non-degenerate diagonal elements:

$$H_{SLIC(S)}^{sec} = \frac{1}{4}\begin{pmatrix} -\omega_{II} & 0 & 0 & 0 & 0 & -\omega_{IS}^{\Delta}/\sqrt{2} & 0 & \omega_{IS}^{\Delta}/\sqrt{2} \\ 0 & 3\omega_{II} & 0 & 0 & 0 & 0 & 0 & 0 \\ 0 & 0 & 3\omega_{II} & 0 & 0 & 0 & 0 & 0 \\ 0 & 0 & 0 & 3\omega_{II} & 0 & 0 & 0 & 0 \\ 0 & 0 & 0 & 0 & -5\omega_{II} & 0 & 0 & 0 \\ -\omega_{IS}^{\Delta}/\sqrt{2} & 0 & 0 & 0 & 0 & -\omega_{II} & 0 & 0 \\ 0 & 0 & 0 & 0 & 0 & 0 & -\omega_{II} & 0 \\ \omega_{IS}^{\Delta}/\sqrt{2} & 0 & 0 & 0 & 0 & 0 & 0 & -\omega_{II} \end{pmatrix} \quad (38)$$

Again, this approximation is justified if $|\omega_{IS}^{\Delta}| \ll |\omega_{II}|$ and $|\omega_{IS}^{\Sigma}| \ll |\omega_{II}|$, i.e. the near-equivalence regime.
The evolution of the system from the initial state in Equation 35 is given by

$$\rho(t) \simeq -\frac{1}{2}p_S^I \, exp\{-iH_{SLIC(S)}^{sec}t'\}\,\mathbf{I_1}\cdot\mathbf{I_2}\,exp\{+iH_{SLIC(S)}^{sec}t'\} \quad (39)$$

where $t = \tau_{SLIC}^{I} + t'$ A *SpinDynamica* calculation shows that this is given by

$$\begin{aligned} \rho(t) \simeq & -\frac{1}{6}p_S^I\left\{2+\cos\left(\frac{\omega_{IS}^{\Delta}t'}{2}\right)\right\}\mathbf{I}_1\cdot\mathbf{I}_2 \\ & -\frac{1}{6}p_S^I\sin^2\left(\frac{\omega_{IS}^{\Delta}t'}{4}\right)(3I_{1z}I_{2z}-\mathbf{I}_1\cdot\mathbf{I}_2) \\ & +\frac{1}{2}p_S^I\sin\left(\frac{\omega_{IS}^{\Delta}t'}{2}\right)(I_{1x}I_{2y}-I_{1y}I_{2x})S_{3z} \\ & +\frac{1}{4}p_S^I\sin\left(\frac{\omega_{IS}^{\Delta}t'}{2}\right)(I_{1z}-I_{2z})S_{3y} \\ & -\frac{1}{4}p_S^I\sin^2\left(\frac{\omega_{IS}^{\Delta}t'}{4}\right)(S_{3x}-4I_{1z}I_{2z}S_{3x}) \end{aligned} \quad (40)$$

The operators in the last term may be written as follows:

$$S_{3x} - 4I_{1z}I_{2z}S_{3x} = 2\left(I_1^{\alpha}I_2^{\beta} + I_1^{\beta}I_2^{\alpha}\right)S_{3x} \quad (41)$$

using the spin-1/2 "polarization operators" $I_j^{\alpha} = 1/2 + I_{jz}$ and $I_j^{\beta} = 1/2 - I_{jz}$. Equation 41 indicates transverse S-spin magnetization with intensity concentrated on the central components of the spectral multiplet, as observed experimentally. The penultimate term in Equation 40 indicates the presence of some out-of-phase terms, which are also observed experimentally.
The optimal S-spin polarization generated along the rotating-frame x-axis is given by:

$$p_x^S(T) = \langle\rho(T) \to P_x^S\rangle = \langle\rho(T) \to P_{3x}\rangle = -P_S^I \quad (42)$$

where $T = \tau_{SLIC}^{I} + \tau_{SLIC}^{S}$. Hence, the S-spin SLIC sequence achieves a theoretical maximum of 100% conversion from I-spin singlet order into S-spin transverse polarization. In an ideal case where the I-spin singlet order to thermal I-spin Zeeman polarization p_{Iz}^{eq} by an I-spin SLIC sequence, the final S-spin polarization is equal to $(2/3)p_{Iz}^{eq}$. If complete I-spin singlet order were generated by a reaction with pure parahydrogen, then 100% S-spin polarization would be achieved in the absence of losses.

Conclusions

In summary, we have shown that it is possible to quantitate the processes underlying parahydrogen-induced polarization experiments by using singlet NMR techniques on thermally polarized samples, allowing the reproducible characterisation and optimisation of the relevant pulse sequences. We have demonstrated two pulse sequence methods for converting the singlet order of one spin species into magnetisation of a different spin species, in the important near-magnetic-equivalence regime, where the difference between the two heteronuclear couplings is much smaller than the homonuclear coupling. The SLIC method achieves the transfer faster than any of the hard-pulse sequences described so far, and is extraordinarily simple and requires minimal rf power. However, the SLIC method is very sensitive to resonance offset, although it might be made more robust with respect to resonance offsets and field inhomogeneity by modulating the amplitude and/or the frequency[26]. The S2hM scheme is a factor $\sim\pi/2$ longer than SLIC, but is much less sensitive to resonance offset than SLIC, and also the other single-channel hard-pulse sequences described in the literature. The power requirements of S2hM may be minimized by employing moderately weak rf pulses. These sequences are likely to be useful at low field, in which case the proton pair may be chemically asymmetric, as is the case for most side-arm hydrogenation molecular targets. This may lead to convenient, cheap, and transportable routes to hyperpolarized materials with a wide range of applications.

Appendix

The solid blue lines in Figures 3 and 4 represent the simulated conversion amplitudes from I-spin (^{1}H) singlet order to S-spin (^{13}C) x-polarization, i.e.

$$a = \langle P_S^I \overset{U}{\to} P_x^S\rangle \quad (43)$$

where the *transformation amplitude* under a unitary propagator U is defined

$$\langle A \overset{U}{\to} B\rangle = \langle UAU^{\dagger} \to B\rangle \quad (44)$$

In Figures 3 and 4, the numerically simulated conversion amplitudes a are plotted against parameters such as time, pulse sequence intervals, rf amplitude, and resonance offset, for various

procedures. In all cases, $a = 1$ represents complete conversion of I-spin singlet polarization into S-spin x-polarization.

Comparison of these curves with experimental measurements is not straightforward. Although the degree of S-spin x-polarization has a direct correspondence with the integrated amplitude of the S-spin NMR signal, no direct NMR measurement of proton singlet polarization is available.

The results of the four different experiments shown in Figure 6 were used to obtain a calibrated measurement of the conversion amplitudes from I-spin singlet order to S-spin x-polarization. All experiments conclude with detection of the S-spin (^{13}C) NMR signal, so that their amplitudes are directly comparable.

Experiment ① involves direct excitation of thermal equilibrium S-spin magnetization and detection of the S-spin signal under I-spin decoupled conditions. The integrated signal amplitude is given by

$$a_{①} = f p_{Sz}^{eq} \tag{45}$$

assuming that enough time is left between transients for full thermal equilibration, as was the case here. The instrumental factor f is common to all four experiments.

Experiment ② involves conversion of thermal equilibrium I-spin magnetization into S-spin magnetization by a refocussed INEPT method, followed by S-spin detection. The INEPT pulse sequence and relevant parameters are given in the Supporting Information.

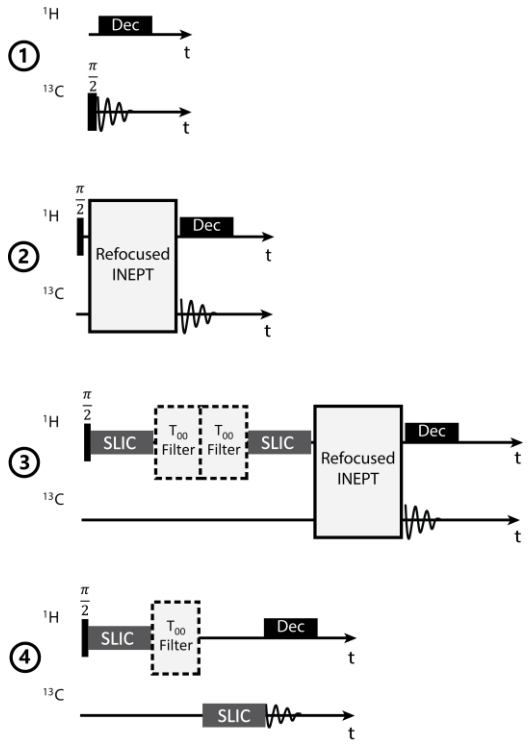

Figure 6: Pulse sequences used to calibrate the conversion amplitude of the ^{13}C SLIC pulse. Details of the INEPT pulse scheme are included in the Supplementary Information.

The integrated signal amplitude is given by

$$a_{②} = f p_{Iz}^{eq} \langle P_z^I \xrightarrow{INEPT} P_z^S \rangle \tag{46}$$

where the INEPT transformation of I-spin polarization into S-spin polarization has a maximal amplitude of 1. The experimental INEPT conversion amplitude may be determined by comparing the signal amplitudes in these two experiments:

$$\langle P_z^I \xrightarrow{INEPT} P_z^S \rangle_{exp} = \frac{p_{Sz}^{eq}}{p_{Iz}^{eq}} \times \frac{a_{②}}{a_{①}} = \frac{\gamma_S a_{②}}{\gamma_I a_{①}} \tag{47}$$

The experimental INEPT conversion amplitude was found to be ~0.67 in our experiments.

Experiment ③ involves generation of I-spin singlet order from thermal I-spin z-polarization using a SLIC scheme, followed by suppression of other density operator components using a T_{00} filter (see Supporting Information for the implementation), followed by another filtration step and reconversion to I-spin z-polarization, INEPT transfer to S-spin polarization, and detection. The integrated signal amplitude is given by

$$a_{③} = f p_{Iz}^{eq} \langle P_z^I \xrightarrow{SLIC^I} P_S^I \rangle \langle P_S^I \xrightarrow{SLIC^I} P_z^I \rangle \langle P_z^I \xrightarrow{INEPT} P_z^S \rangle \tag{48}$$

where the T_{00} filters have been implicitly included in $SLIC^I$, for the sake of brevity.

The transformation amplitude brackets under the I-spin SLIC sequence are related as follows:

$$\langle P_S^I \xrightarrow{SLIC^I} P_z^I \rangle \simeq \frac{\|P_S^I\|^2}{\|P_z^I\|^2} \langle P_z^I \xrightarrow{SLIC^I} P_S^I \rangle \tag{49}$$

This may be proved as follows: For brevity, denote P_S^I as A, and P_z^I as B. Assuming purely unitary evolution under a Hamiltonian H, the "forward" transformation amplitude may be written

$$\langle A \xrightarrow{U} B \rangle = \frac{\mathrm{Tr}\{B^\dagger U A U^\dagger\}}{\|B\|^2} = \frac{\mathrm{Tr}\left\{B^\dagger exp\{-iH\tau\}\, A\, exp\{+iH\tau\}\right\}}{\|B\|^2} \tag{50}$$

where H includes the I-spin rf field and the interaction terms. By using the invariance of the trace to cyclic permutation, and assuming that the operators A and B are Hermitian, we get:

$$\langle A \xrightarrow{U} B \rangle = \frac{\mathrm{Tr}\left\{A^\dagger exp\{+iH\tau\}\, B\, exp\{-iH\tau\}\right\}}{\|B\|^2} \tag{51}$$

The antilinear operator K_0, as defined by Weitekamp[42] may be applied to all terms inside the trace. This operator takes the complex conjugate of all terms, reversing the sign of any y-angular momentum operators, but leaving x and z-operators invariant. The operators A and B are invariant to transformation by K_0. Since the coupling Hamiltonian H^0 is also invariant under transformation by K_0, and the SLIC scheme only employs rf fields of phase 0, the total Hamiltonian H is also invariant under transformation by K_0. We get:

$$\langle A \xrightarrow{U} B \rangle = \frac{\mathrm{Tr}\left\{K_0 A^\dagger K_0^\dagger exp\{K_0(+iH\tau)K_0^\dagger\}\, K_0 B K_0^\dagger\, exp\{K_0(-iH\tau)K_0^\dagger\}\right\}}{\|B\|^2}$$

$$= \frac{\mathrm{Tr}\left\{A^{*\dagger} exp\{-iH^*\tau\}\, B^*\, exp\{+iH^*\tau\}\right\}}{\|B\|^2}$$

$$= \frac{\mathrm{Tr}\{A^\dagger U B U^\dagger\}}{\|B\|^2}$$

$$= \langle B \xrightarrow{U} A \rangle \frac{\|A\|^2}{\|B\|^2}$$

(52)

Equation 49 follows by assuming that the non-unitary dissipative terms have a roughly equivalent effect in both directions. The ratio of the operator norms is

$$\frac{\|P_S^I\|^2}{\|P_z^I\|^2} = \frac{3}{2}$$

(53)

and hence

$$a_{③} \simeq \frac{3}{2} f p_{Iz}^{eq} \left| \langle P_z^I \xrightarrow{SLIC^I} P_S^I \rangle \right|^2 \langle P_z^I \xrightarrow{INEPT} P_z^S \rangle$$

(54)

This leads to

$$\frac{a_{③}}{a_{②}} \simeq \frac{3}{2} \left| \langle P_z^I \xrightarrow{SLIC^I} P_S^I \rangle \right|^2$$

(55)

The experimental amplitude ratio was found to be $a_{③}/a_{②} = 0.24$ from which we deduce an experimental transformation amplitude $\langle P_z^I \rightarrow P_S^I \rangle \simeq 0.4$ for the conversion of thermal I-spin z-polarization into I-spin singlet order by the I-spin SLIC sequence, followed by T_{00} filtering. This should be compared with the theoretical maximum of $2/3 \simeq 0.67$.

Experiment ④ involves generation of I-spin singlet order from thermal I-spin z-polarization using a I-spin SLIC scheme, followed by a T_{00} filter and conversion into S-spin polarization using a S-spin SLIC scheme.

The integrated signal amplitude is given by

$$a_{④} = f p_{Iz}^{eq} \langle P_z^I \xrightarrow{SLIC^I} P_S^I \rangle \langle P_S^I \xrightarrow{SLIC^S} P_z^S \rangle$$

(56)

The transformation amplitude for the S-spin SLIC sequence may therefore be derived from the experimental amplitudes as follows:

$$\langle P_S^I \xrightarrow{SLIC^S} P_z^S \rangle \simeq \sqrt{\frac{3}{2}} \frac{\gamma_S a_{④}}{\gamma_I a_{①}} \sqrt{\frac{a_{②}}{a_{③}}}$$

(57)

These are the experimental points plotted in Figures 3 and 4.

Acknowledgements

This research was supported by the Engineering and Physical Sciences Research Council (UK), (grant numbers EP/N002482/1, EP/L505067/1 and EP/M508147/1), and the ERASMUS and Marie-Skłodowska programs of the European Community (655864-SingMet). We thank Jean-Nicolas Dumez and Karel Kouril for discussions of theory, and Benno Meier for experimental help.

1. S. J. Nelson et al., Metabolic Imaging of Patients with Prostate Cancer Using Hyperpolarized [1-13C]Pyruvate, Sci. Transl. Med., 2013, **5**, 198
2. C. R. Bowers, D. P. Weitekamp, Parahydrogen and synthesis allow dramatically enhanced nuclear alignment, J. Am. Chem. Soc., 1987, **109**, 5541
3. F. Reineri, T. Boi, S. Aime, ParaHydrogen Induced Polarization of 13C carboxylate resonance in acetate and pyruvate, Nat. Commum., 2014, **6**, 5858
4. F. Reineri et al., Use of Labile Precursors for the Generation of Hyperpolarized Molecules from Hydrogenation with Parahydrogen and Aqueous-Phase Extraction, Angew. Chem. Int. Ed., 2011, **50**, 7350
5. E. Cavallari et al., Effects of Magnetic Field Cycle on the Polarization Transfer from Parahydrogen to Heteronuclei through Long-Range J-Couplings, J. Phys. Chem. B., 2015, **119**, 10035
6. M. Haake, J. Natterer, J. Bargon, Efficient NMR Pulse Sequences to Transfer the Parahydrogen-Induced Polarization to Hetero Nuclei, J. Am. Chem. Soc., 1996, **118**, 8688
7. K. Golman et al., Parahydrogen-induced polarization in imaging: Subsecond 13C angiography, Magn. Reson. Med., 2001, **46**, 1
8. H. Jóhannesson, O. Axelsson, M. Karlsson, Highly polarized nuclear spin systems and dipolar interactions in NMRTransfer of para-hydrogen spin order into polarization by diabatic field cycling, C. R. Phys., 2004, **5**, 315
9. M. Goldman, H Johannesson, Conversion of a proton pair para order into 13C polarization by rf irradiation, for use in MRI, C. R. Phys., 2005, **6**, 575
10. M. Goldman et al., Hyperpolarization of 13C through order transfer from parahydrogen: A new contrast agent for MRI, J. Magn. Reson. Imaging, 2005, **23**, 153
11. S. Kadlecek et al., Optimal transfer of spin-order between a singlet nuclear pair and a heteronucleus, J. Magn. Reson., 2010, **205**, 9
12. A. N. Pravdivtsev et al., Robust conversion of singlet spin order in coupled spin-1/2 pairs by adiabatically ramped RF-fields, J. Magn. Reson., 2016, 273, 56-64
13. A. S. Kiryutin et al., Exploiting adiabatically switched RF-field for manipulating spin hyperpolarization induced by parahydrogen, J. Chem. Phys., 2015, 143, 234203
14. A. Pravdivtsev et al., Highly Efficient Polarization of Spin-1/2 Insensitive NMR Nuclei by Adiabatic Passage through Level Anticrossings, J. Phys. Chem. Lett., 2014, 5, 3421-3426
15. S. Bär et al., On the spin order transfer from parahydrogen to another nucleus, J. Magn. Reson., 2012, **225**, 25
16. Cai et al., Efficient Transformation of Parahydrogen Spin Order into Heteronuclear Magnetization, J. Phys. Chem. B., 2013, **117,** 1219
17. V. A. Norton, Efficient generation of hyperpolarized molecules utilizing the scalar order of parahydrogen, PhD thesis, California Institute of Technology, 2010
18. S. F. Glöggler, Para-hydrogen perspectives in hyperpolarized NMR, J. Colell, S. Appelt, J. Magn. Reson., 2013, **235**, 130
19. M. H. Levitt, Singlet Nuclear Magnetic Resonance, Annu. Rev. Phys. Chem., 2012, **63**, 89
20. M. Carravetta, O. G. Johannessen, M. H. Levitt, Beyond the T_1 Limit: Singlet Nuclear Spin States in Low Magnetic Fields, Phys. Rev. Lett., 2004, **92**, 153003
21. M. Carravetta, M. H. Levitt, Long-Lived Nuclear Spin States in High-Field Solution NMR, J. Am. Chem. Soc., 2004, **126**, 6228
22. G. Pileio, M. Carravetta, M. H. Levitt, Storage of nuclear magnetization as long-lived singlet order in low magnetic field, Proc. Natl. Acad. Sci., 2010, **107**, 17135
23. R. Sarkar., P. R. Vasos, G. Bodenhausen, Singlet-State Exchange NMR Spectroscopy for the Study of Very Slow Dynamic Processes, J. Am. Chem. Soc., 2007, **129**, 328
24. A. S. Kiryutin et al., Manipulating spin hyper-polarization by means of adiabatic switching of a spin-locking RF-field, Phys. Chem. Chem. Phys., 2013, **15**, 14248
25. S. J. DeVience, R. L. Walsworth, M. S. Rosen, Preparation of Nuclear Spin Singlet States Using Spin-Lock Induced Crossing, Phys. Rev. Lett., 2013, **111**, 173002

26. T. Theis et al., Composite and shaped pulses for efficient and robust pumping of disconnected eigenstates in magnetic resonance, J. Chem. Phys., 2014, **140**, 14201
27. T. Theis et al., LIGHT-SABRE enables efficient in-magnet catalytic hyperpolarization, J. Magn. Reson., 2014, **248**, 23
28. Y. Zhang et al., Singlet lifetime measurements in an all-proton chemically equivalent spin system by hyperpolarization and weak spin lock transfers, Phys. Chem. Chem. Phys., 2015, **17**, 24370
29. Y. Zhang et al., Limits in Proton Nuclear Singlet-State Lifetimes Measured with para-Hydrogen-Induced Polarization, Chem. Phys. Chem., 2016, **17**, 2967
30. M. C. D. Tayler, M. H. Levitt, Singlet nuclear magnetic resonance of nearly-equivalent spins, Phys. Chem. Chem. Phys., 2011, **13**, 5556
31. Y. Feng et al., Storage of Hydrogen Spin Polarization in Long-Lived $^{13}C_2$ Singlet Order and Implications for Hyperpolarized Magnetic Resonance Imaging, J. Am. Chem. Soc., 2013, **135**, 9632
32. Y. Feng, R. M. Davis, W. S. Warren, Accessing long-lived nuclear singlet states between chemically equivalent spins without breaking symmetry, Nat. Phys., 2012, **8**, 831
33. M.C.D. Tayler, M. H. Levitt, Accessing Long-Lived Nuclear Spin Order by Isotope-Induced Symmetry Breaking, J. Am. Chem. Soc., 2013, **135**, 2120
34. Levitt, M.H. SpinDynamica code for Mathematica, programmed by Malcolm H. Levitt, with contributions by Jyrki Rantaharju, Andreas Brinkmann, and Soumya Singha Roy, available at www.spindynamica.soton.ac.uk
35. M. H. Levitt, R. Freeman, Compensation for pulse imperfections in NMR spin-echo experiments, J. Magn. Reson., 1981, **43**, 65
36. R. R. Ernst, G. Bodenhausen, A. Wokaun, Principles of Nuclear Magnetic Resonance in One and Two Dimensions, 1987
37. J. Jeener, Superoperators in Magnetic Resonance, Adv. Magn. Reson. 10 (1982) 1
38. A. Bornet et al., Long-Lived States of Magnetically Equivalent Spins Populated by Dissolution-DNP and Revealed by Enzymatic Reactions, 2014, **51**, 17113
39. D. Mammoli et al., Hyperpolarized para-Ethanol, 2015, **119**, 4048
40. Y. Feng et al., Long-lived polarization protected by symmetry, J. Chem. Phys., 2014, **141**, 134307
41. M. H. Levitt, Symmetry constraints on spin dynamics: Application to hyperpolarized NMR, J. Magn. Reson., 2016, **262**, 91-99
42. D. P. Weitekamp, Time-Domain Multiple Quantum NMR, Adv. Magn. Reson., 1983, **11**, 111274